IEEE Photonics Journal
An IEEE Photonics Society Publication

Open Access

Underwater Wireless Optical Communications Using Silicon Photo-Multipliers

Volume 9, Number 4, August 2017

Mohammad-Ali Khalighi
Tasnim Hamza
Salah Bourennane
Pierre Léon
Jan Opderbecke

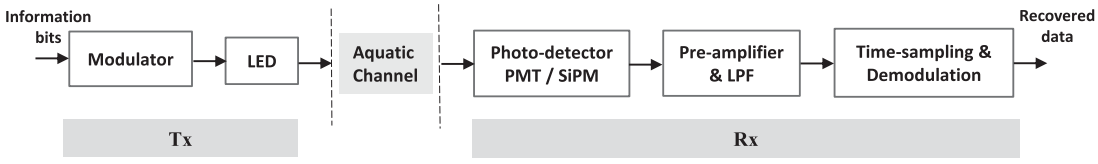

DOI: 10.1109/JPHOT.2017.2726565
1943-0655 © 2017 IEEE

IEEE photonics SOCIETY

IEEE

Underwater Wireless Optical Communications Using Silicon Photo-Multipliers

Mohammad-Ali Khalighi,[1] **Tasnim Hamza,**[1,2] **Salah Bourennane,**[1] **Pierre Léon,**[2] **and Jan Opderbecke**[2]

[1]Aix Marseille University, CNRS, Centrale Marseille, Institut Fresnel, Marseille, France
[2]IFREMER Research Institute, La Seyne-sur-Mer 83500, France

DOI:10.1109/JPHOT.2017.2726565

Manuscript received July 7, 2017; accepted July 10, 2017. Date of publication July 14, 2017; date of current version July 27, 2017. This work was supported in part by the French PACA (Provence, Alpes, Côte d'Azur) Regional Council. Corresponding author: Mohammad-Ali Khalighi (e-mail: Ali.Khalighi@fresnel.fr).

Abstract: We study the use of Silicon photo-multipliers (SiPMs) for underwater wireless optical communications (UWOC) and discuss their main interests and drawbacks, compared with photo-multiplier tubes. This comparison is mainly based on practical considerations regarding system implementation and the attainable link span. Presenting an appropriate model for signal attenuation in water and considering the simple On–Off keying modulation, we bring clearance on the real interest of using an SiPM in the UWOC context. We also elucidate the main drawbacks of these components in practice, in particular, regarding the limitation on the transmission data rate, as well as the nonlinear distortion caused on the received signal in relatively short ranges, where the signal intensity is too large.

Index Terms: Underwater wireless optical communications, Silicon photo-multiplier, single-photon avalanche diode, photo-multiplier tube, underwater optical channel.

1. Introduction

Underwater wireless optical communications (UWOC) are well known as a promising technology for high data rate transmission in aquatic media [1]–[3]. As concerns the choice of optoelectronic components, at the transmitter (Tx), light-emitting diodes (LEDs) are mostly used for the reasons of lower cost and beam alignment simplicity due to their relatively wider beam compared to laser diode counterparts. Concerning the choice of the photo-detector (PD) at the receiver (Rx), the classical PIN PDs are unsuitable for UWOC, given the high attenuation of the optical channel. Avalanche photo-diodes (APDs) are interesting due to their inherent gain and have been used in several experimental and theoretical works, e.g., [4], [5]. Photo-multiplier tubes (PMTs), on the other hand, appear to be a more suitable choice and have drawn particular attention thanks to their very high gain, and consequently, their high sensitivity to very low intensity levels [3], [4]. They are, for instance, used in the BlueComm underwater modems developed by Sonardyne [6]. However, they are bulky and expensive, require high voltage for operation, are sensitive to magnetic fields, and can be easily damaged by exposure to high-intensity light [7], [8].

Recently, Silicon photo-multipliers (SiPMs), also known as multi-pixel photon counters, have emerged as quite promising PDs when working with very low intensity levels down to a single photon [9]. An SiPM is composed of a number of APDs biased above the breakdown voltage. As compared

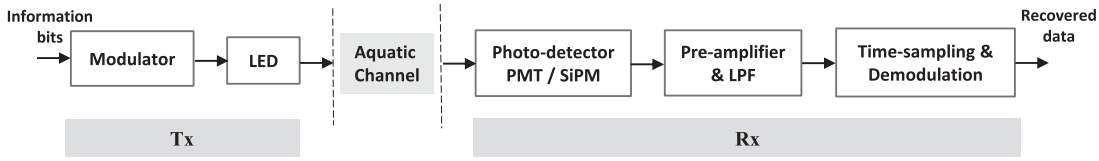

Fig. 1. General block diagram of an UWOC link employing a PMT or an SiPM.

with PMTs, SiPMs offer several advantages such as low operation voltage, insensitivity to magnetic fields, and mechanical robustness. The feasibility of using SiPMs in optical communications was firstly shown in [10], [11]. In [12] these components were used for the design of very sensitive receivers for plastic optical fiber long-haul links. Also, [13]–[15], investigated SiPMs for low-power visible light communications (VLC), e.g., for down-hole monitoring applications, and an experimental work in [16] demonstrated a 200 Mbps VLC link using a single-photon avalanche diode (SPAD)-based Rx. Considering a single SPAD with a quite large lens at the Rx and high power emitters, it was claimed in [17] that link spans over 500 m can be attained in clear waters (but this conclusion could be of limited practical interest due to the excessive system parameters considered). Recently, we presented a novel prototype of an optical modem based on SiPM receivers in [18] and showed the practical advantage of using these components through a number of lab experiments and sea trials under different water turbidity conditions.

Our aim in this paper is to investigate the interest of employing SiPMs in UWOC applications by making reasonable assumptions on the link parameters and using available PDs. To go farther, we also study the limitations on the transmission rate that arise from bandwidth (BW) limitation of the SiPM. In fact, in a previous work [19], we assumed a flat frequency response for the SiPM. Here, we revisit this assumption and show to which extent the maximum tolerable data transmission rate can be constrained and when this BW limitation can necessitate channel equalization at the Rx. Meanwhile, although it is not the main purpose of this work, in contrast to [19], we present a more appropriate model for the optical channel intensity loss when using an LED as emitter, which has rarely been clarified in the literature, to the best of our knowledge.

The rest of the paper is organized as follows. In Section 2, we present the UWOC system description and the channel attenuation model. The description of SiPM function and its modeling are provided in Section 3. Performance evaluation of the communication link is explained in Section 4 where we specify the components' parameters and explain how to take their BW limitation into account. Next, we present a set of numerical results in Section 5 to evaluate the link performance for relatively moderate and high transmission rates, and Section 6 concludes the paper.

2. Mathematical Modeling of the Received Signal Intensity

Fig. 1 shows a typical UWOC link where an LED is used as the emitting device, and a PMT or an SiPM is used at the Rx side. We model the LED radiation pattern P_t by a generalized Lambertian model with azimuthal symmetry. Denoting the transmit power by P_{Tx}, we have:

$$P_t = P_{Tx} \frac{m+1}{2\pi} \cos^m(\theta), \quad \text{W/sr}, \tag{1}$$

where $\theta \in [0, \pi/2]$ is the angle of irradiance of the LED, and m is its Lambertian order given by $m = -\ln(2)/\ln\left(\cos(\theta_{1/2})\right)$ with $\theta_{1/2}$ being the Tx semi-angle at half-power.

2.1 Optical Signal Attenuation in Water

Light propagation underwater is subject to high attenuation due to absorption and scattering that depend on the properties of water and the light beam. Concerning the latter, the attenuation profile depends on the optical source type, i.e., whether the beam is collimated or not. Basically, the exact

channel attenuation is described by the radiative transfer equation, which can be solved analytically or numerically [20], or approximated through Monte Carlo simulations [21]. Alternatively, a simple approximate exponential attenuation model can be used, which provides a sufficiently accurate estimate of the optical power in clear waters where absorption is predominant [5], [21]. However, this underestimates the received intensity for relatively high water turbidities, because of neglecting multiple scattering of photons. Since our aim here is to study the interest of using SiPMs in UWOC systems, we settle for this simple formulation of the channel loss.

The classical exponential attenuation model is that of the Beer-Lambert (BL) [20] according to which, the intensity loss at a distance Z is given by $\exp(-cZ)$, where the wavelength-dependent attenuation coefficient c is in units of m^{-1}. This model can be used in the case of a narrow collimated light beam [20], e.g.,, when the emitter is a laser diode. When a diffuse light source (i.e., an uncollimated beam) is used at the Tx, like an LED, c does not characterize the light propagation adequately, and should be replaced by the so-called diffuse attenuation coefficient that we denote by K_d [20], [22]. We denote the channel loss as:

$$L_{ch} = \exp(-K_d Z). \tag{2}$$

The point is now to determine K_d for a given water type. For this, we have resorted to similar studies on modeling solar light penetration in water [22], [23]. Indeed, solar radiations can be modeled as a diffuse light source for which a set of measured profiles of irradiance attenuation versus depth can be found in [20], [22], [24]–[26] for various water types. In addition, there exist several predictive bio-optical models in the literature [27]–[30] to estimate K_d for a given wavelength λ and Chlorophyll concentration C_{cl}, in addition to some earlier experimental data by Jerlov [20]. Here, we consider the model of [28] that is regarded as more reliable.

It is worth mentioning that like C_{cl}, K_d varies with depth D [26]. Here, for the sake of simplicity, we assume that we work at depths far from the sea bottom and surface (e.g., $D > 60$ m [25]), where K_d converges to an asymptotic value [20]. For instance, for the case of clear waters, with the typical $C_{cl} = 0.5$ mg/m^3 [20] and $\lambda = 470$ nm (blue), we obtain $K_d \approx 0.08\,m^{-1}$.

2.2 Received Signal

Based on the presented channel model, and assuming perfect Tx-Rx alignment, the captured power by the Rx, denoted by P_{Rx}, is given by [31]:

$$P_{Rx} = P_t \exp(-K_d Z)\,\frac{A_{PD}}{Z^2}, \tag{3}$$

where A_{PD} is the physical area of the PD. As shown in Fig. 1, the PD's output photo-current is converted to voltage by means of a high-speed low-noise trans-impedance (TZ) amplifier and low-pass filter (LPF) prior to time sampling and demodulation. Assuming that our system operates in relatively deep waters, we neglect the effect of background radiations [23]. For the case of using a PMT, the formulations of the received signal and noise are similar to that of an APD [32].

3. Silicon Photomultipliers

An SiPM consists in an array of APDs which are biased at Geiger mode, i.e., above the breakdown voltage. Each APD is then commonly called a SPAD. When a photon heats the SPAD sensitive area, an avalanche breakdown is occurred, which generates a pulse at the SPAD output. The SPAD can hence be considered as a single photon counter [14], which is connected to an active or passive quenching device that halts the Geiger discharge. The SiPM output C_{ph} is the sum of the photon counts $c_{ph}(i)$ of its constituting SPADs of number N_{SPAD}:

$$C_{ph} = \sum_{i=1}^{N_{SPAD}} c_{ph}(i). \tag{4}$$

We assume that the SiPM has an ideal photon counting behavior and model its photo-detection by a Poisson distribution [15]. That is:

$$\Pr(C_{\text{ph}} = k) = \exp(-\mu)\,\frac{\mu^k}{k!}, \tag{5}$$

where Pr(.) denotes probability and μ stands for the average photon count and is expressed as a function of the captured optical power by the Rx as follows [13]:

$$\mu = \left(\frac{\Upsilon_{\text{PDE}}\,P_{\text{Rx}}}{E_{\text{ph}}} + f_{\text{DCR}}\right)(1 + P_{\text{AP}} + P_{\text{CT}})\,T. \tag{6}$$

Here, T denotes the symbol duration and $E_{\text{ph}} = \hbar c/\lambda$ is the energy of a photon, with $\hbar$ the Planck constant and c the speed of light. Also, Υ_{PDE} is the photon detection efficiency, which is defined as the product of the quantum efficiency, the fill factor (ratio of the active area to the total physical area of the SiPM), and the probability that a detected photon generates an avalanche; P_{AP} is the probability of after-pulsing, which consists in the re-trigger of a SPAD by trapped carriers at its output from the previous avalanche; P_{CT} is the probability of cross-talk, which occurs when an avalanching SPAD initiates an avalanche in another one; and f_{DCR} is the dark count rate, which results from the breakdown of a SPAD due to thermally generated electrons.

Another key parameter of an SiPM is its dead-time (also called recovery time) τ_{d}, which is the time required by a SPAD to recharge. Indeed, the SPAD is unable to detect a newly arriving photon during τ_{d}. This SiPM *saturation* can cause a non-linear distortion (NLD) on the received signal [15], which depends on the type of the quenching device used. In the case of passive quenching (PQ), the extra photon arrivals, although uncounted, cause the SPAD to collapse (i.e., be parallelized) by extending the dead-time. This is not the case for active quenching (AQ) SiPMs, where the incoming photons during τ_{d} are not counted and consequently do not prolong the dead-time.

In the following, we will focus on PQ SiPMs. Indeed, among the commercially available SiPMs, AQ devices have a very limited number of SPADs (e.g., 8 for the ID Quantique SiPMs [33]), compared to PQ devices (e.g., 10998 for SensL B-series 30020 SiPMs [34]), and are more expensive. Now, for the incoming number of photons given by (6), the average output count of the SiPM (i.e., the actually measured photons) during a symbol duration T is [15]:

$$\mu_{\text{PQ}} = \mu\,\exp\left(-\frac{\mu\,\tau_{\text{d}}}{T\,N_{\text{SPAD}}}\right). \tag{7}$$

The maximum number of photons before the saturation of the SiPM can be readily obtained as:

$$\mu_{\text{PQ,max}} = \frac{T\,N_{\text{SPAD}}}{e\,\tau_{\text{d}}}. \tag{8}$$

The photon counting formulation presented here is quite compatible with the block diagram of Fig. 1 which shows a practical Rx implementation. In fact, the number of generated photo-electrons is proportional to the photo-current at the SiPM output. This conversion is sometimes represented by a so-called photon-to-amplitude equalizer [15].

4. Performance Evaluation

4.1 Signal Transmission

We consider a typical UWOC link employing intensity modulation with direct detection based on uncoded non-return-to-zero On-Off keying (OOK) [35]. We denote by P_0 and P_1 the transmitted optical power for bits '0' and '1', and define the extinction ratio EXT as P_0/P_1. Signal detection for the case of a PMT being rather classical, we focus here on an SiPM-based Rx. We denote by $\mu_{\text{PQ},0}$ and $\mu_{\text{PQ},1}$ the average SiPM output corresponding to bits '0' and '1', respectively. For signal demodulation, we use the optimal detection threshold μ_{th} minimizing the error probability. Assuming that the number of received photons is large enough, we can approximate the corresponding Poisson distributions by Gaussian. For instance, for the case of an On symbol, the Poisson distribution with

TABLE 1
PD Parameter Specification

SiPM parameter		PMT parameter	
Photon detection efficiency, Υ_{PDE}	24%	Load resistance, R_L	1 KΩ
Surface area	9 mm^2	Number of dynodes, n_d	9
Fill factor	48%	Collection efficiency, α	≈ 1
Dark count rate, f_{DCR}	6.6 MHz	Anode dark current (at $\sim 17^\circ$C)	4 nA
Dead-time, τ_d	100 ns	Quantum efficiency	25%
Number of SPADs, N_{SPAD}	10998	Gain, G_{PMT}	9.5×10^6
Probability of cross-talk, P_{CT}	0.03%	Diameter	28 mm
Probability of after-pulsing, P_{AP}	0.2%	Noise figure	≈ 1

parameter $\mu_{PQ,1}$ is approximated by a Gaussian with mean and variance equal to $\mu_{PQ,1}$. Setting the same error probability for '0' and '1' bits, $\Pr(\mu_{PQ} > \mu_{th}|\text{'0'}) = \Pr(\mu_{PQ} \leq \mu_{th}|\text{'1'})$, we get:

$$\mu_{th} = \sqrt{\mu_{PQ,0}\, \mu_{PQ,1}} \tag{9}$$

Note that this equation is valid under the approximation of Poisson distributions with Gaussian. The reader is referred to [17] for the exact expression of μ_{th} in the general case.

4.2 Parameter Specification

At the Tx side, we consider a blue LED at $\lambda = 470$ nm e.g., the NICHIA NSPB510AS model [36] (the SiPM has its highest sensitivity on this λ). The LED optical emitting power is set to 1 W and its half-angle to $\theta_{1/2} \approx 10^\circ$, corresponding to $m \approx 45$, which can be readily obtained using appropriate optics. At the Rx side, we consider a SensL B-series MicroSB 30020 fast, blue-sensitive SiPM [34] whose detailed parameters are given in Table 1. No lens is used at the Rx to insure a large Rx field-of-view (FOV), which is important in practice in order to alleviate and beam misalignment problems [37]. For the sake of comparison, we also consider a Hamamatsu R12896 nine-stage PMT [38], with parameters given in Table 1. The PMT gain depends on the number n_d of dynodes (photo-electron multiplication stages) and the collection efficiency of the first dynode α: $G_{PMT} = \alpha\, \delta^{n_d}$ [8], where δ denotes the multiplication factor of each dynode. We should notice the much larger PD active area of the PMT, compared with the SiPM.

We consider two cases of clear and coastal waters for which we set K_d to 0.08 m^{-1} (see Subsection 2.1) and 0.5 m^{-1}, respectively. For the latter case, we used a C-star transmissometer (from WET Labs [39]) in Ifremer Institute docks close to Toulon, France.

4.3 Modeling Bandwidth Limitation

We consider the normalized equivalent aggregate channel impulse response (IR) as $h_{eq}(t) = h_{LED}(t) * h_{ch}(t) * h_{SiPM}(t)$, where h_{LED}, h_{ch} and h_{SiPM} denote the IRs of the LED, the aquatic channel, and the SiPM, respectively, and $*$ denotes convolution. It is well known that the UWOC channel can be considered as frequency non-selective for most practical link scenarios [21]. Thus, $h_{ch}(t) = L_{ch}\, \delta(t)$ where L_{ch} is given by (2) and $\delta(.)$ is the Dirac function. As concerns the LED, we model it by a 1st-order RC LPF of normalized IR $h_{LED}(t) = e^{-2\pi f_{c,L} t}$, where $f_{c,L}$ denotes the LED 3-dB cut-off frequency [40]. The frequency response was measured experimentally as such data are not provided in the data-sheet. To measure the LED cut-off frequency, we used a fast Silicon PIN

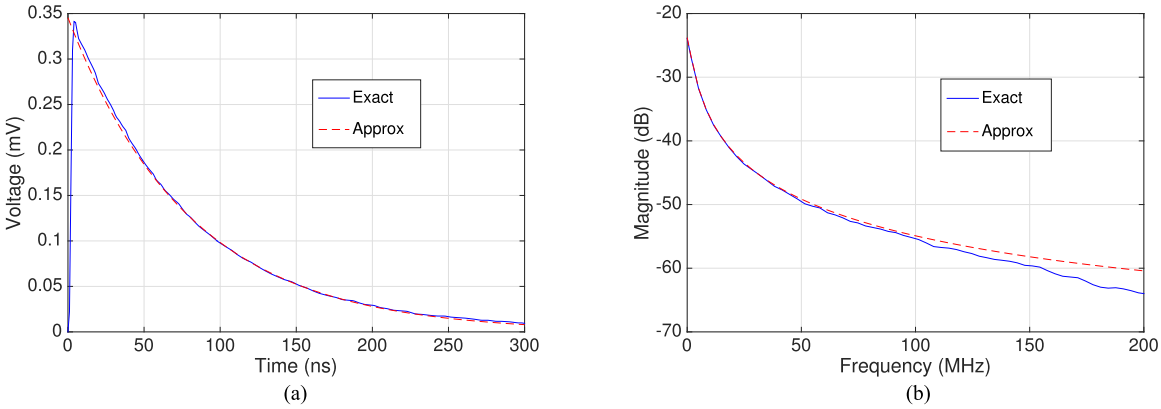

Fig. 2. SensL MicroSB-30035 SiPM: (a) IR, (b) frequency response. Exact and approximate (1st-order LPF) characteristics.

PD (OSD1-5T model with high blue sensitivity and low dark current [41]). The measured $f_{c,L}$ was around 10 MHz.

For the SiPM, apart from the limitation of dead-time (see Section 3), we could be still limited by the device BW, i.e., for symbol rates $R < 1/\tau_d$. Following the same approach as for the LED, we model the SiPM by a 1st-order LPF of IR $h_{SiPM}(t) = e^{-2\pi f_{c,S} t}$ with $f_{c,S}$ denoting the 3-dB modulation BW. We have presented the normalized IR [34] and the corresponding frequency response in Fig. 2, where $f_{c,S} \approx 2$ MHz. The IR is in fact the readout voltage of the SiPM to a 40 ps laser pulse firing about 2.5% of the micro-cells [34]. The output pulse has a rise time of a few ns and a fall time of several 100 ns; we can consider it as an "impulse response" then. From Fig. 2, we see that this 1st-order LPF approximation is quite accurate for frequencies up to 100 MHz. It is worth mentioning that we reasonably assume that the TZ pre-amplifier (see Fig. 1) has a quite faster response than the PD (see [34], recommended readout circuit specifications).

5. Numerical Results

5.1 Comparison Between PMT and SiPM

Let us first consider the simple case of EXT$=0$. We have presented in Fig. 3 plots of bit-error-rate (BER) versus range for PMT- and PQ-SiPM-based Rxs for clear and coastal waters. We have not presented the BER for too short ranges where the SiPM will be parallelized (see next subsection). If we set the target BER to 10^{-3}, the achieved range is about 126 and 26.5 m for the PMT-based Rx and 66 and 16.2 m for the SiPM-based system, in clear and coastal waters, respectively. (A BER of about 10^{-3} for an uncoded system is considered as sufficiently low that can be reduced to less than 10^{-9} by error correction coding [42].) The larger active area of the PMT is the main reason of its better performance. Obviously, the SiPM cannot compete with the PMT in terms of the attainable link span. Despite this, it keeps the undebatable practical advantages that we explained in Section 1.

5.2 Effect of EXT Parameter

Let us know focus on the SiPM operation while considering a non-zero EXT, because in practice we cannot completely switch off the LED (i.e., set EXT to 0) at a high rate. We have presented BER plots versus Z in Fig. 4 for different EXT values. For not-too-short Z (here, $Z > 30$ m), increasing EXT obviously results in a reduced detection signal-to-noise ratio (SNR), and hence, a degraded BER performance for a given Z. If we set the target BER to 10^{-3}, the attainable link range decreases by increasing EXT: it is about 66, 62.5, 53, and 37.5 m for EXT $= 0,\ 0.3\,,\ 0.5$, and 0.8, respectively.

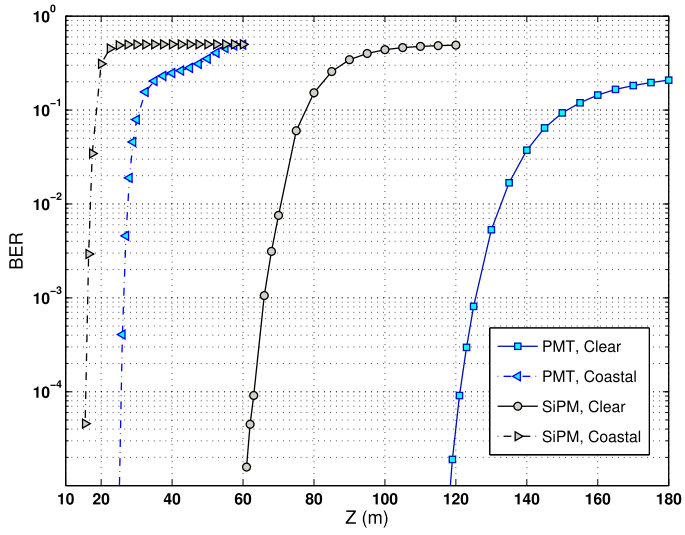

Fig. 3. BER versus link distance Z for PMT- and PQ-SiPM-based receivers. $P_1 = 1$ W, uncoded OOK with EXT $= 0$, $R = 1$ Mbps; $K_d = 0.08\,\mathrm{m}^{-1}$ for clear waters and $0.5\,\mathrm{m}^{-1}$ for coastal waters.

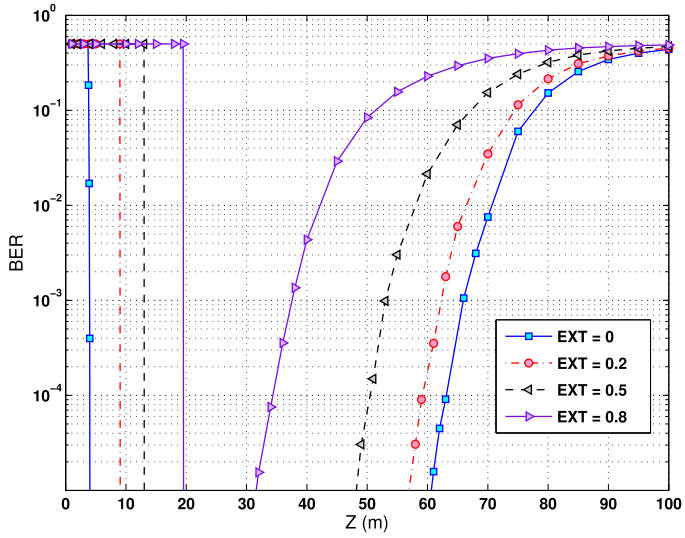

Fig. 4. BER versus link distance for the PQ-SiPM-based Rx, uncoded NRZ-OOK modulation with different EXT. $P_t = 1$ W, $R = 1$ Mbps, clear ocean waters.

We have also shown in the figure the effect of SiPM NLD when the input signal intensity is too large, i.e., at short Z. Indeed, from (3) and (6), by decreasing Z, the average number μ of arriving photons at the Rx increases, and hence the number of actually measured photons μ_{PQ}. When we enter the saturation regime, μ_{PQ} can be much smaller than μ. Even, it makes that $\mu_{\mathrm{PQ},1}$ becomes much smaller than $\mu_{\mathrm{PQ},0}$. Consequently, given μ_{th} in (9), the detected bit will be inversed and we get a BER of one. As this can be quite confusing, we have preferred to set the BER to 0.5 at the saturation limit, because in any way the Rx cannot operate correctly under such conditions. For a larger EXT, the bits '0' will be increasingly affected by the NLD and the minimum tolerable Z increases. The saturation limit is about 4, 9, 13, and 19.5 m for EXT $= 0$, 0.3 , 0.5, and 0.8, respectively. Overall, the range of Z in which the system can function appropriately narrows with increasing EXT. Lastly, notice from (8) that the larger N_{SPAD} and the lower R, the shorter will be the link range that the system can tolerate.

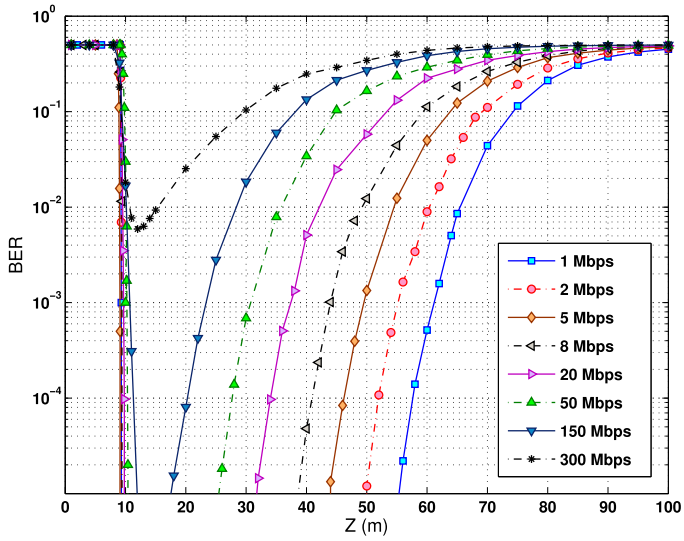

Fig. 5. BER versus Z for different data rates. PQ-SiPM-based Rx, uncoded NRZ-OOK with $P_1 = 1$ W and EXT $= 0.2$, clear ocean waters. LED and SiPM are assumed to have infinite modulation BW.

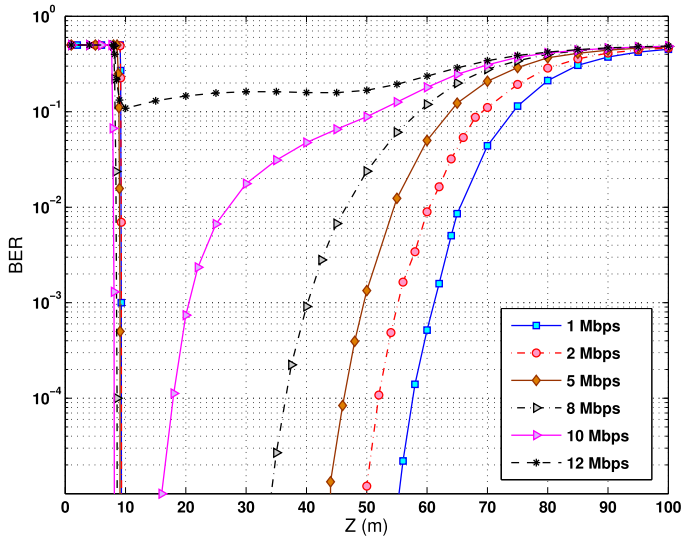

Fig. 6. BER versus Z for different data rates. PQ-SiPM-based Rx, uncoded NRZ-OOK with $P_1 = 1$ W and EXT $= 0.2$, clear ocean waters. $f_{c,L} = 10$ and $f_{c,S} = 2$ MHz.

5.3 Performance for High Data Rates

Lets now investigate the limitation in terms of the transmission rate. Basically, given the principal dead-time limitation (see Section 3), for symbol rates larger than $1/\tau_d$, the SiPM does not have enough time to completely recharge (i.e., to drain off the carriers). Additionally, as explained in Subsection 4.3, the limited BW of the SiPM can affect the link performance at high R. Note that we implicitly assume that we use adequate pulse shaping satisfying the Nyquist criterion.

Let us first assume that the LED and SiPM have infinite modulation BWs. To see the limitation caused by τ_d, we have shown the BER plots versus Z in Fig. 5 for EXT $= 0.2$ and different data rates of $R = 1, 2, 5, 8, 20, 50, 150, 300$ Mbps. We notice that the maximum attainable range for a given target BER decreases with increasing R, which was expected. Indeed, decreasing T below τ_d

results in a reduced effective detection SNR since there will be a smaller difference between $\mu_{PQ,0}$ and $\mu_{PQ,1}$. Nevertheless, although $\tau_d = 100$ ns, this limitation does not make the SiPM to collapse totally until a symbol rate of about 350 Mbps (not shown in the figure).

Now we do consider the BW limitation of the LED and SiPM. Since the LED has a larger BW, the limitation arises principally from the SiPM. We have shown in Fig. 6 BER plots for $R = 1$, 2, 5, 8, and 12 Mbps and under the same conditions as for Fig. 5. Note that we do not perform any equalization at the Rx; our aim is just to see to which extent the data rate is constrained. As before, the attainable maximum range for a given target BER decreases with increasing R. This decrease is more noticeable in this case because the ISI resulting from the limited BW of the components is deteriorating signal detection. The data rate is practically limited to about 10 Mbps with a significant penalty in the attainable link range. Obviously, this ISI can be mitigated by performing channel equalization at the Rx, see for instance [43], [44].

6. Conclusion

We investigated the interest of using SiPMs in UWOC systems. Compared with PMTs, albeit offering shorter transmission ranges (due mainly to the typically smaller detector active area), as well as suffering from NLD at very short ranges and from a higher noise level (dark count rate, cross talk, and after pulsing), these components present undebatable advantages for practical implementation of such links. Considering the classical uncoded OOK modulation, we investigated the effect of the extinction ratio and the impact on the link performance by taking into account the NLD caused by a PQ-SiPM in short link ranges. We also elucidated the actual limitation on the maximum transmission rate caused by the SiPM operation as well as its modulation BW. We showed that the latter parameter can be much more constraining when no channel equalization is done at the Rx. Our on-going research focuses on investigating the performance of these components under background light influence and in high turbidity waters.

References

[1] M. A. Khalighi, C. J. Gabriel, L. M. Pessoa, and B. Silva, "Underwater visible light communications, channel modeling and system design," in *Visible Light Communications: Theory and Applications*. Boca Raton, FL, USA: CRC Press, 2017, pp. 337–372.

[2] M. A. Khalighi, C. Gabriel, T. Hamza, S. Bourennane, P. Léon, and V. Rigaud, "Underwater wireless optical communication; recent advances and remaining challenges," in *Proc. Int. Conf. Transparent Opt. Netw.*, Graz, Austria, Jul. 2014, pp. 1–4.

[3] F. Hanson and S. Radic, "High bandwidth underwater optical communication," *Appl. Opt.*, vol. 47, no. 2, pp. 277–283, Jan. 2008.

[4] B. Cochenour, L. Mullen, and J. Muth, "Temporal response of the underwater optical channel for high-bandwidth wireless laser communications," *IEEE J. Ocean. Eng.*, vol. 38, no. 4, pp. 730–742, Oct. 2013.

[5] M. Doniec, M. Angermann, and D. Rus, "An end-to-end signal strength model for underwater optical communications," *IEEE J. Ocean. Eng.*, vol. 38, no. 4, pp. 743–757, Oct. 2013.

[6] "Sonardyne product: BlueComm underwater optical modem." [Online]. Available: https://www.sonardyne.com/product/bluecomm-underwater-optical-communication-system/

[7] P. Lacovara, "High-bandwidth underwater communications," *Mar. Technol. Soc. J.*, vol. 42, no. 1, pp. 93–102, Mar. 2008.

[8] *Photomultiplier Tubes, Basics and Applications*, 3a ed. Hamamatsu Photonics K.K., Electron Tube Division, TOTH9001E03a Japan, 2007.

[9] SensL, "Introduction to the silicon photomultiplier, Technical Note," 2011. [Online]. Available: http://www.sensl.com/

[10] I. Alsolami, D. Chitnis, D. C. O'Brien, and S. Collins, "Broadcasting over photon-counting channels via multiresolution PPM: Implementation and experimental results," *IEEE Commun. Lett.*, vol. 16, no. 12, pp. 2072–2074, Dec. 2012.

[11] G. Zhang, C. Yu, C. Zhu, and L. Liu, "Feasibility study of multi-pixel photon counter serving as the detector in digital optical communications," *Elsevier Optik J.*, vol. 124, no. 22, pp. 5781–5786, 2013.

[12] D. Chitnis and S. Collins, "A SPAD-Based photon detecting system for optical communications," *J. Lightw. Technol.*, vol. 32, no. 10, pp. 2028–2034, May 2014.

[13] Y. Li, S. Videv, M. Abdallah, K. Qaraqe, M. Uysal, and H. Haas, "Single photon avalanche diode (SPAD) VLC system and application to downhole monitoring," in *Proc. Global Commun. Conf.*, Austin, TX, USA, Dec. 2014, pp. 2108–2113.

[14] Y. Li, M. Safari, R. Henderson, and H. Haas, "Optical OFDM with single-photon avalanche diode," *IEEE Photon. Technol. Lett.*, vol. 27, no. 9, pp. 943–946, May 2015.

[15] Y. Li, M. Safari, R. Henderson, and H. Haas, "Nonlinear distortion in SPAD-based optical OFDM systems," in *Proc. Global Commun. Conf. Workshop Opt. Wireless Commun.*, San Diego, CA, USA, Dec. 2015, pp. 1–6.
[16] D. Chitnis *et al.*, "A 200 Mb/s VLC demonstration with a SPAD based receiver," in *Proc. IEEE Summer Top. Meeting Ser.*, Nassau, Bahamas, Jul. 2015, pp. 226–227.
[17] C. Wang, H. Y. Yu, and Y. J. Zhu, "A long distance underwater visible light communication system with single photon avalanche diode," *IEEE Photon. J.*, vol. 8, no. 5, Oct. 2016, Art. no. 7906311.
[18] P. Léon *et al.*, "A new underwater optical modem based on highly sensitive silicon photo-multipliers," in *Proc. IEEE OCEANS Conf.*, Aberdeen, U.K., Jun. 2017.
[19] T. Hamza, M. A. Khalighi, S. Bourennane, P. Léon, and J. Opderbecke, "On the suitability of employing silicon photo-multipliers for underwater wireless optical communication links," in *Proc. Int. Symp. Commun. Syst., Netw. Digit. Signal Process.*, Prague, Czech Republic, Jul. 2016, pp. 1–5.
[20] C. Mobley, *Light and Water: Radiative Transfer in Natural Waters*. New York, NY, USA: Academic, 1994.
[21] C. Gabriel, M. A. Khalighi, S. Bourennane, P. Léon, and V. Rigaud, "Monte-Carlo-based channel characterization for underwater optical communication systems," *IEEE/OSA J. Opt. Commun. Netw.*, vol. 5, no. 1, pp. 1–12, Jan. 2013.
[22] J. W. Giles and I. N. Bankman, "Underwater optical communication systems. Part 2: Basic design considerations," *Proc. Mil. Commun. Conf.*, Oct. 2005, vol. 3, pp. 1700–1705.
[23] T. Hamza, M. A. Khalighi, S. Bourennane, P. Léon, and J. Opderbecke, "Investigation of solar noise impact on the performance of underwater wireless optical communication links," *Opt. Exp.*, vol. 24, no. 22, pp. 25 832–25 845, Oct. 2016.
[24] J. Tyler, "Radiance distribution as a function of depth in an underwater environment," *Bulletin Scripps Inst. Oceanogr.*, vol. 7, no. 5, pp. 363–412, 1960.
[25] S. Q. Duntley, "Light in the sea," *J. Opt. Soc. Amer.*, vol. 53, no. 2, pp. 214–233, Feb. 1963.
[26] E. B. C. Mobley and C. Roesler, *Ocean Optics Web Book*, 2016. [Online]. Available: http://www.oceanopticsbook.info/
[27] R. C. Smith and K. S. Baker, "Optical properties of the clearest natural waters (200–800 nm)," *Appl. Opt.*, vol. 20, no. 2, pp. 177–184, Jan. 1981.
[28] B. Woźniak and V. N. Pelevin, "Optical classifications of the seas in relation to phytoplankton characteristics," *Oceanologia*, vol. 31, pp. 25–55, Dec. 1991.
[29] R. W. Austin and T. J. Petzold, "Spectral dependence of the diffuse attenuation coefficient of light in ocean waters," *Opt. Eng.*, vol. 25, no. 3, Mar. 1986, Art. no. 253471.
[30] A. Morel, "Optical modeling of the upper ocean in relation to its biogenous matter content (case I waters)," *J. Geophys. Res.*, vol. 93, no. C9, pp. 10749–10768, Sep. 1988.
[31] J. M. Kahn and J. R. Barry, "Wireless infrared communication," *Proc. IEEE*, vol. 85, no. 2, pp. 265–298, Feb. 1997.
[32] F. Xu, M. A. Khalighi, and S. Bourennane, "Impact of different noise sources on the performance of PIN- and APD-based FSO receivers," in *Proc. 11th Int. Conf.Telecommun. (ConTEL)*, Graz, Austria, Jun. 2011, pp. 211–218.
[33] ID Quantique, "ID150 VIS 8 channel SPAD: Miniature 8-channel photon counter for OEM applications," 2010. [Online]. Available: http://www.idquantique.com
[34] SensL, "b-series fast, blue-sensitive silicon photomultiplier sensors datasheet and user manual," 2013. [Online]. Available: http://www.sensl.com/
[35] C. Gabriel, M. A. Khalighi, S. Bourennane, P. Léon, and V. Rigaud, "Investigation of suitable modulation techniques for underwater wireless optical communication," in *Proc. Int. Workshop Opt. Wireless Commun.*, Pisa, Italy, Oct. 2012, pp. 1–3.
[36] NICHIA Corporation, "Specifications for blue LED: NSPB510AS." [Online]. Available: http://www.nichia.co.jp, accessed: Jul. 2017.
[37] C. Gabriel, M. A. Khalighi, S. Bourennane, P. Léon, and V. Rigaud, "Misalignment considerations on point-to-point underwater wireless optical links," in *Proc. IEEE Oceans Conf.*, Bergen, Norway, Jun. 2013, pp. 1–5.
[38] Hamamatsu, "R3896, R12896 high sensitivity multialkali photocathode 28 mm (1-1/8 inch) diameter, 9-stage, side-on type." [Online]. Available: http://www.hamamatsu.com, accessed: Jul. 2017.
[39] WET Labs, "C-Star Transmissometer," Jun. 2010. [Online]. Available: http//wetlabs.com/cstar
[40] S. Long, M. A. Khalighi, M. Wolf, Z. Ghassemlooy, and S. Bourennane, "Performance of carrier-less amplitude and phase modulation with frequency domain equalization for indoor visible light communications," in *Proc. 4th Int. Workshop Opt. Wireless Commun.*, Sep. 2015, pp. 16–20.
[41] Centronic Co., "Silicon photodetector OSD1-5T datasheet." [Online]. Available: http://www.centronic.co.uk, accessed: July 2017.
[42] A. H. Azhar, T. A. Tran, and D. O'Brien, "A Gigabit/s indoor wireless transmission using MIMO-OFDM visible-light communications," *IEEE Photon. Technol. Lett.*, vol. 25, no. 2, pp. 171–174, Jan. 2013.
[43] M. A. El-Shimy, and S. Hranilovic, "Binary-input non-line-of-sight solar-blind UV channels: Modeling, capacity and coding," *IEEE/OSA J. Opt. Commun. Netw.*, vol. 4, no. 12, pp. 1008–1017, Dec. 2012.
[44] C. Gong and Z. Xu, "Channel estimation and signal detection for optical wireless scattering communication with inter-symbol interference," *IEEE Trans. Wireless Commun.*, vol. 14, no. 10, pp. 5326–5337, Oct. 2015.